Field Measurements of Duration-Limited Growth of Wind-Generated Ocean Surface Waves at Young Stage of Development*

PAUL A. HWANG AND DAVID W. WANG

Oceanography Division, Naval Research Laboratory, Stennis Space Center, Mississippi

(Manuscript received 13 May 2003, in final form 13 April 2004)

ABSTRACT

The issue of duration-limited growth of wind-generated waves is of importance to wave studies. Most analytical solutions for wind waves are given in time rather than fetch domain. Numerical modeling of wave development is also often conducted in temporal evolution mode. Experimental data of duration-limited growth, however, are rare and do not cover a wide range of the wave development stage. As a result, theorists and modelers have to rely on fetch-limited evolution data, converting them into duration-limited conditions on the basis of some assumptions. During one of the field experiments of wind wave measurements, a dataset was obtained that is almost ideal for duration-limited wave growth analysis. The dataset extends the range of coverage in dimensionless time of the existing database by about one order of magnitude. The results of analysis provide strong support for the relation of space–time conversion for rendering the fetch-limited growth functions to duration-limited growth functions. Quantitative discussions on the development rate of fetch and duration growth are presented.

1. Introduction

Two classes of ocean wave measurements are of great importance to researchers interested in surface wave generation under steady wind forcing. The first class is the fetch-limited growth condition, under which the wave development is limited by the available spatial coverage upwind of the measurement location. The spatial limitation is typically caused by the presence of land mass; therefore, fetch-limited wave measurements are usually conducted in coastal regions or lakes with winds blowing from land to water. Over the years, there have been several successful field experiments reported (e.g., Burling 1959; Hasselmann et al. 1973; Kahma 1981; Donelan et al. 1985; Dobson et al. 1989; Young and Verhagen 1996; Young 1997; Babanin and Soloviev 1998). Extensive reviews and analyses on these datasets have been given (e.g., Kahma and Calkoen 1992, 1994; Young 1999).

The second class is the duration-limited growth condition, under which the wave development is limited by the temporal duration of the steady wind event acting on the water surface. Ideally, the water stays calm until the sudden start of a steady wind reaching rapidly to a set speed. These initial and boundary conditions rarely occur in nature. The wind direction may stay steady for a long period of time but ramping up of wind speed from zero to a set speed usually takes some time. Also, in the open ocean, background swell is almost always present. It is no wonder that reports of duration-limited wave data are very scarce. Young (1999) presents an extensive review of fetch- and duration-limited wave growth studies. The only duration-limited datasets cited are Sverdrup and Munk (1947), Bretschneider (1952a,b), and Darbyshire (1959), as compiled by Wiegel (1961). DeLeonibus and Simpson (1972) report field data that contain duration growth information. All of these data are obtained at later stages of wave development with dimensionless time t_* greater than about 8000.

Considering the difficulty of acquiring field measurements of duration-limited wave growth, conversion equations of simple power-law fetch-limited growth functions to duration-limited growth functions have been proposed before (e.g., Bretschneider 1952a,b; Mitsuyasu and Rikiishi 1978). Comparing with existing duration-limited data (rather scattered), the agreement between the converted functions and measurements is encouraging. In this paper, we introduce a higher-order data-fitting technique that yields fetch-limited growth functions in second-order power-law functions. The exponent of the power-law function (hereinafter referred to as the development rate) is not a constant but varies

* U.S. Naval Research Laboratory Contribution Number JA/7330-03-0012.

Corresponding author address: Dr. Paul A. Hwang, Oceanography Division, Naval Research Laboratory, Stennis Space Center, MS 39529-5004.
E-mail: paul.hwang@nrlssc.navy.mil

TABLE 1. Coefficients and exponents of the fetch-limited growth functions.

	A_{ex1}	a_{ex1}	α_0	α_1	α_2
$e_*(x_*)$	6.191×10^{-7}	0.8106	−17.6158	1.7645	−0.0647
	$A_{\omega x1}$	$a_{\omega x1}$	β_0	β_1	β_2
$\omega_*(x_*)$	11.86	−0.2368	3.0377	−0.3990	0.0110

with dimensionless fetch. The second-order functions improve agreement between fitted functions and measured data especially at very large and very small dimensionless fetches. The conversion from fetch-limited to duration-limited growth functions for the first- and second-order power-law functions is presented in section 2. The analysis highlights the daunting challenge facing the experimentalists seeking to obtain field measurements of duration-limited wave growth data at young stage of wave development. For example, based on the second-order power-law growth functions, for a nominal wind speed of 10 m s^{-1}, at dimensionless time (t_*) equal to 1000, the expected significant wave height (H_s) is 0.18 m and peak wave period (T_p) is 1.48 s. At $t_* = 100$, the expected H_s and T_p are 0.019 m and 0.49 s. Furthermore, the duration for wave development to reach $t_* = 1000$ is 1020 s; and to reach $t_* = 100$, the duration drops to 102 s for 10 m s^{-1} wind speed.

Recently an experiment was carried out to measure fetch growth of small-scale wind-generated waves at the early stage of wave development in a sheltered bay to reduce background wave contamination. Postprocessing of the data reveals that one of the sequences of measurements is an almost ideal duration-limited growth case. The experimental procedures and data analysis are described in section 3. Those measurements expand the range of the available duration-limited database by about one order of magnitude to $t_* \approx 1000$. The analysis results also confirm the validity of space–time conversion to transform the fetch-limited growth functions to the duration domain. Section 4 presents summary and concluding remarks.

2. Fetch- and duration-limited growth functions

a. Fetch-limited condition

The fetch-limited growth functions in the deep water condition can be expressed by the following two equations:

$$e_* = A_{ex} x_*^{a_{ex}} \quad \text{and} \tag{1a}$$

$$\omega_* = A_{\omega x} x_*^{a_{\omega x}}, \tag{1b}$$

where $e_* = \sigma^2 g^2/U_{10}^4$, $\omega_* = \omega_p U_{10}/g$, $x_* = xg/U_{10}^2$, σ^2 is the variance of the surface elevation, g is the gravitational acceleration, U_{10} is the neutral wind speed at 10-m elevation, ω_p is the angular frequency of the spectral peak wave component, and x is fetch. For the simple power-law representation, the coefficients A and exponents a are constant. Extensive discussions on the simple power-law fetch-limited growth functions have been given before (e.g., Kahma and Calkoen 1994; Young 1999). The simple power-law functions describe the fetch-limited growth reasonably well over a broad range of the dimensionless fetch between approximately 3×10^2 and 10^4.

The exponents of the power-law functions represent the development rate of wave energy and wave period with increasing fetch. In the very short and very long fetches, the measured data deviate from the simple power-law functions, reflecting the fact that the wave development rate is not a constant. At an early stage of development (shorter dimensionless fetch), experimental data suggest a steeper rate of development. Similarly, at later stages of wave development, the wave growth slows down. The variation of development rate can be estimated by employing a higher-order fitting to the experimental data. To the second order, the resulting power-law functions are given by

$$e_* = A_{ex2} x_*^{a_{ex2}} \quad \text{and} \tag{2a}$$

$$\omega_* = A_{\omega x2} x_*^{a_{\omega x2}}, \tag{2b}$$

with the coefficients and exponents derived from second-order polynomial fitting of $\ln e_*(\ln x_*)$ and $\ln\omega_*(\ln x_*)$; that is,

$$\ln e_* = \alpha_0 + \alpha_1 \ln x_* + \alpha_2 (\ln x_*)^2 \quad \text{and} \tag{3a}$$

$$\ln\omega_* = \beta_0 + \beta_1 \ln x_* + \beta_2 (\ln x_*)^2. \tag{3b}$$

The fetch-dependent coefficients A_2 and a_2 are related to α_0, α_1, α_2, β_0, β_1, and β_2 by (detail in appendix A)

$$A_{ex2} = e^{\alpha_0} x_*^{-\alpha_2 \ln x_*}, \tag{4a}$$

$$a_{ex2} = \alpha_1 + 2\alpha_2 \ln x_*, \tag{4b}$$

$$A_{\omega x2} = e^{\beta_0} x_*^{-\beta_2 \ln x_*}, \quad \text{and} \tag{5a}$$

$$a_{\omega x2} = \beta_1 + 2\beta_2 \ln x_*. \tag{5b}$$

From analyzing five different datasets of field measurements conducted in steady wind conditions (Burling 1959; Hasselmann et al. 1973; Donelan et al. 1985; Dobson et al. 1989; Babanin and Soloviev 1998), the coefficients and exponents of the first- and second-order power-law growth functions are obtained (Table 1).

b. Duration-limited condition

For wave energy propagation, space and time can be connected by

$$\int_0^t dt = \int_0^x \frac{dx}{C_{gx}}, \qquad (6)$$

where C_{gx} is the downwind component of the wave group velocity. The equation can be expressed in dimensionless form

$$\int_0^{t_*} dt_* = \int_0^{x_*} \frac{\omega_*}{R}\, dx_*, \qquad (7)$$

where $t_* = tg/U_{10}$, $R = C_{gx}/C_p$, and C_p is the phase speed of the wave spectral peak component. For a monochromatic wave train, $R = 0.5$. For wind seas, field measurements by Yefimov and Babanin (1991) show that $R = 0.4$. Substituting (1b) to (7), for the simple power-law case (constant exponents), the space–time conversion equation is

$$t_* = \frac{A_{\omega x}}{R(a_{\omega x} + 1)} x_*^{a_{\omega x}+1} \quad \text{or}$$

$$x_* = \left[\frac{R(a_{\omega x} + 1)}{A_{\omega x}} t_*\right]^{1/(a_{\omega x}+1)}. \qquad (8)$$

The duration-limited growth functions become

$$e_* = A_{et} t_*^{a_{et}} \quad \text{and} \quad \omega_* = A_{\omega t} t_*^{a_{\omega t}}, \qquad (9)$$

with

$$A_{et} = A_{ex}\left[\frac{R(a_{\omega x} + 1)}{A_{\omega x}}\right]^{a_{et}}, \qquad a_{et} = \frac{a_{ex}}{a_{\omega x} + 1}, \qquad (10)$$

$$A_{\omega t} = A_{\omega x}[R(a_{\omega x} + 1)]^{a_{\omega x}}, \quad \text{and} \quad a_{\omega t} = \frac{a_{\omega x}}{a_{\omega x} + 1}. \qquad (11)$$

For second-order power-law functions (fetch-dependent exponents), substitution of (2b) [with coefficient and exponent in (5)] to (7) gives (see appendix A)

$$t_* = \frac{\exp[\beta_0 - (\beta_1 + 1)^2/4\beta_2]\ \mathrm{erf}i[(\beta_1 + 1 + 2\beta_2 x_*)/(2\sqrt{\beta_2})]}{2\sqrt{\beta_2}}, \qquad (12)$$

where erf$i$ is the imaginary error function, related to the error function erf by erf$i(z) = i$ erf(iz).The conversion equation (12) proves to be cumbersome. An approximation is adopted by substituting (4) and (5) for A_{ex}, a_{ex}, $A_{\omega x}$, and $a_{\omega x}$ in (10) and (11) to compute the second-order duration-limited wave growth.

c. *Quantitative discussions*

With the substitution of the numerical values listed in Table 1 for the coefficients and exponents, the fetch-limited and duration-limited growth functions are graphed in Fig. 1a for $\omega_*(x_*)$, $e_*(x_*)$ and Fig. 1b for $\omega_*(t_*)$ and $e_*(t_*)$. Applying the one-to-one relation among ω_*, e_*, and x_* or t_*, the pairs of growth functions in fetch and duration can also be represented by $e_*(\omega_*)$, as shown in Fig. 1c. Because ω_* is also the inverse wave age, this expression can be interpreted as the wave energy growth as a function of wave age. Furthermore, because fetch and duration disappear from the $e_*(\omega_*)$ expression, this function eliminates one of the major error sources in wave growth analysis. For the simple (first order) power-law functions, $e_*(\omega_*)$ calculated from fetch laws and duration laws are identical, as expected. For the second-order power-law functions, the solution of $e_*(\omega_*)$ from duration laws is slightly different from that calculated from the fetch laws, also as expected due to the approximation described in the last paragraph. The two second-order solutions of $e_*(\omega_*)$ are quite close, however.

As illustrated in the figure, the development rate in time is considerably higher than the development rate in space. For example, based on the first-order fitting (Table 1), the spatial development rate is 0.81 for $e_*(x_*)$ and -0.24 for $\omega_*(x_*)$. The temporal development rate is calculated from (10) and (11) to be 1.06 for $e_*(t_*)$ and -0.31 for $\omega_*(t_*)$. The fetch-dependent development rate can be calculated from α_1, α_2 and β_1, β_2 using (4)–(5) for spatial development and (10)–(11) for temporal development.

Based on the above analysis, we can estimate the conditions of wave growth at young stage in terms of fetch, duration, expected wave height, and wave period for a given wind speed. For example, Table 2 lists the numerical values of these parameters for $t_* = 100$ and 1000 and $x_* = 100$ and 1000.

These numbers illustrate the very demanding challenge in acquiring measurements of duration growth of young waves in the field, in addition to the luck needed to encounter the rare occurrences of a steady wind event with sharp rise to a constant wind speed in a quiescent background environment.

3. Field measurements and data analysis

a. *Wind and wave measurement system*

An experiment was conducted in St. Andrew Bay near Panama City, Florida, on 11 and 12 October 2001 to measure small-scale ocean surface waves. All sensors were mounted on a free-drifting surface-following buoy,

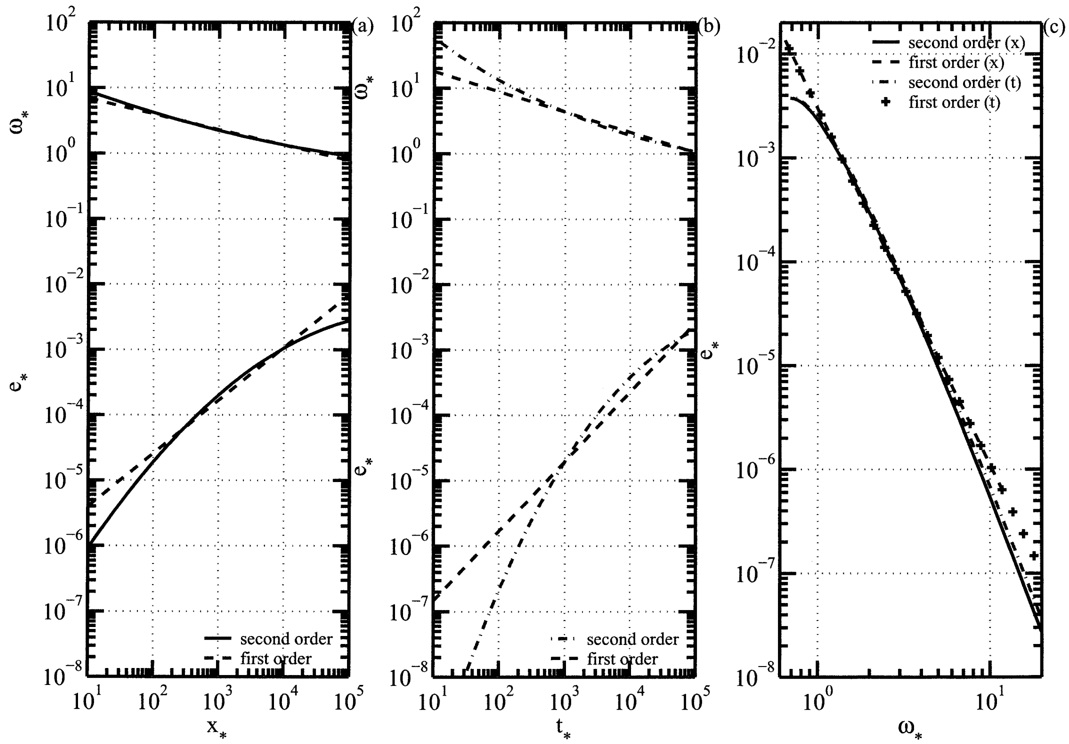

FIG. 1. (a) Fetch-limited growth, $e_*(x_*)$ and $\omega_*(x_*)$, expressed as first-order and second-order power-law functions, (b) conversion of fetch-limited to duration-limited growth functions $e_*(t_*)$ and $\omega_*(t_*)$, and (c) growth laws expressed as $e_*(\omega_*)$.

similar in design to an earlier version of the scanning slope sensing buoy system described by Hwang et al. (1996). Surface wind velocity is measured by an ultrasonic anemometer (Handar 425A) at 1-Hz sampling rate. This wind sensor is mounted 1.4 m above the mean water level. Surface waves are measured by two linear arrays of wave gauges aligned in the crosswind and upwind directions. Each array has 20 fast response capacitance wave gauges (1-mm-diameter thin wires) using the design by Chapman and Monaldo (1991). The spatial interval between the wire gauges is 0.0508 m. Effects from buoy translation and angular motions on wave measurements are corrected using the output from motion sensors (accelerometers and tilt sensors) mounted on the buoy, following the approach proposed by Hanson et al. (1997).

TABLE 2. Examples of fetch, duration, significant wave height, and peak wave period at young stages of wave development for U_{10} = 10 m s^{-1}.

	Fetch		
x_*	x (m)	H_s (m)*	T_p (s)*
100	1020	0.21 (0.18)	1.61 (1.53)
1000	10204	0.53 (0.58)	2.78 (2.56)
	Duration		
t_*	t (s)	H_s (m)	T_p (s)
100	102	0.05 (0.02)	0.72 (0.49)
1000	1020	0.18 (0.18)	1.48 (1.48)

* For H_s and T_p, numbers in parentheses are from second-order power-law functions, and numbers not in parentheses are from first-order power-law functions.

The technical details of the capacitance wave gauges have been documented in the technical report by Chapman and Monaldo (1991). The response of the wire gauges is very linear over the 1-m design range. In the original design as deployed in St. Andrew Bay, the regression coefficient of the response function is almost constant for salinity greater than about 4 psu. The response function becomes nonlinear in water with lower salinity. (To deploy the system in fresher water, ground wires stretching parallel to the capacitance wave gauges are added. Empirically, it is found that spacing of about 0.02 m between each ground wire and wave gauge produces satisfactory results of linear response.) Figure 2a shows the laboratory calibration of the wave gauges at three salinity levels. At 26 psu, the average slope (millimeters per digitization step) with one standard deviation is 0.219 $\pm$ 0.0032 for the upwind array and 0.221 $\pm$ 0.0025 for the crosswind array. At 14 psu, those numbers are 0.219 $\pm$ 0.0033 and 0.224 $\pm$ 0.0026, respectively. The salinity in St. Andrew Bay, where the ship stayed, ranges from 31.6 to 32.2 psu and about 34.2 psu in the coastal water outside the bay. The calibration results in 26 psu water are used for the data analysis of this experiment.

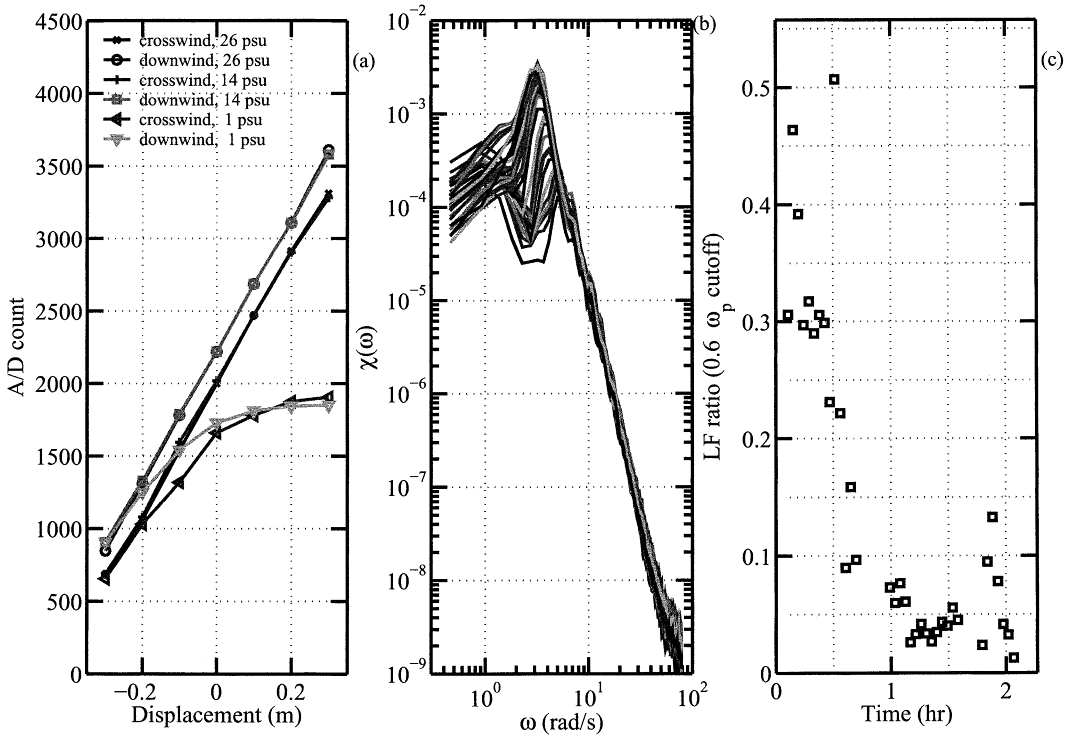

FIG. 2. (a) Laboratory calibration of the wave gauge arrays at different salinity levels, (b) the wave spectra $\chi(\omega)$ measured by the wave gauge array, and (c) the variance ratio between the low-frequency components ($\omega < 0.6\omega_p$) and the total.

The analog-to-digital circuit digitizes the wave data with 12-bit resolution for 10 volts that covers the 1-m design range (design value is 2.44×10^{-4} m per digitization step, actual value is 2.2×10^{-4} m per digitization step). The sample rate can be either 25 or 50 Hz. For the 25-Hz sample rate used in the present experiment, the noise floor due to digitization was calculated to be 7.7×10^{-11} m^2/(rad s^{-1}) and for 50 Hz it is 3.9×10^{-11} m^2/(rad s^{-1}). The noise floor from examining the spectrum of wave gauge output in ambient conditions is 2×10^{-10} m^2/(rad s^{-1}), which represents the overall noise of the wave gauge array system. The full set of 35 frequency spectra, $\chi(\omega)$, of the present experiment is shown in Fig. 2b. The spectral peaks are usually at least six to seven orders of magnitude above the noise floor. There is clear presence of low-frequency oscillations due to ambient motions in the bay water. The wave variance presented in the paper excludes the low-frequency (LF) components ($\omega < 0.6\omega_p$), which represent background contamination. The fraction of LF components is computed by the variance ratio of the LF components to the total (Fig. 2c). The large influence of background waves at the early stage of wave development is clearly illustrated by the large fraction of low-frequency wave energy. The presence of background oscillations represents the largest error source for the analysis of wind wave growth at the early stage of development.

During the period of the experiment, the wind was steady and mainly from the south-southeast. The buoy is deployed in free drift near the southeast corner of the bay. There are a total of nine sets of wind and wave data acquired during this two-day period. The duration of each set is between 1200 and 2400 s. The wind and wave parameters are computed from short data segments. Each data segment is about 164 s (4096 wave samples at 25-Hz sampling rate), containing about 80–100 significant waves (see next paragraph). Only the wave data from the central five wire gauges of the upwind array are used for the discussions in this paper. The degree of freedom is 24 for the spectra from individual wire gauges and 120 for the average wave spectra combining five wire gauges. The full set of 35 wave spectra is shown in Fig. 2b. Neutral wind speed at 10-m height (U_{10}) and at an elevation one-half of the peak wavelength ($U_{\lambda/2}$) are calculated from the measured wind speed at 1.4-m height combined with the measured humidity, air and water temperatures, applying the method developed by Liu et al. (1979) to obtain the dynamic roughness z_0 and making use of the logarithmic wind speed profile.

b. Field deployment and experimental conditions

Figure 3 shows the area map of the experimental site. On 12 October the wave gauge array buoy is released

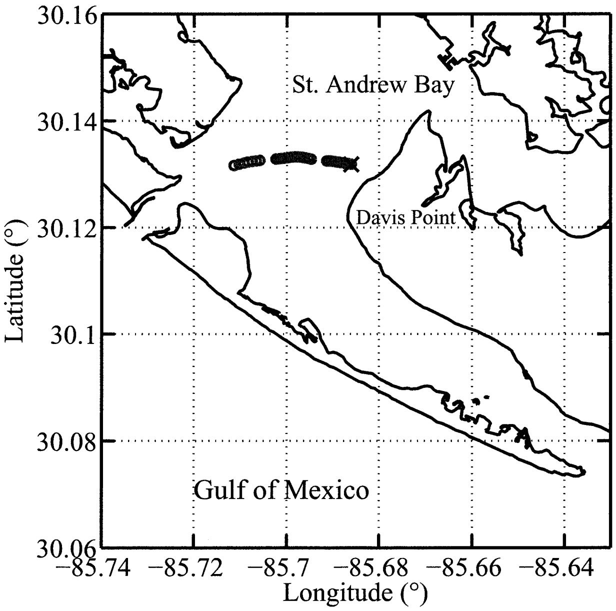

FIG. 3. Area map of the experimental site in St. Andrew Bay. The buoy was released into water at the location marked ‘‘×.’’ The buoy trajectory for 11–12 Oct 2001 is shown by ‘‘○.’’

into water at the location marked with ‘‘×.’’ The prevailing wind is from the south-southeast (162° from north). The experiment is originally planned for fetch-limited data acquisition, but the strong ebb tide soon takes the buoy into the open area of the bay. The trajectory of the buoy from the GPS recording on board the buoy is shown by the overlapping circles in the map. The recorded wave development becomes more duration limited rather than fetch limited. [The significant wave height based on fetch-limited condition for the average wind speed of 8.3 m s^{-1} (Fig. 4) is 0.13, 0.29 and 0.34 m, respectively, for fetches of 0.5, 4 and 6 km estimated from the map. The measured significant wave height starts at 0.1 m (of which about 50% is contributed by background oscillations; Fig. 2c), reaches about 0.27 at 5400 s, and reaches 0.31 m near the end of the 2-h duration (Table 3 and Fig. 4). It is judged that in the first 1.5 h, the data are dominantly duration limited, but they become influenced by limited fetch for the last 0.5 h.] The sensors on the buoy collect data in bursts of usually 40 min long. Restarting of the data acquisition sequence is activated manually through a remote control radio link. Altogether three sets of data on this day are collected. Because the drifting speed near the bay entrance increases rapidly (Fig. 3), the third set is 20 min long. As a result, 100 min of data are collected over 124-min duration.

The average wind speed ($U_{\lambda/2}$), wind direction (θ_u), significant wave height (H_s), peak wave period (T_p), and bulk Richardson number (Ri_b) (Donelan 1990) for the duration of experiment are shown in Fig. 4. The mean wind speed with one standard deviation is 8.3 ± 0.5 m s^{-1}, and the wind direction is 162 ± 6°. The air–

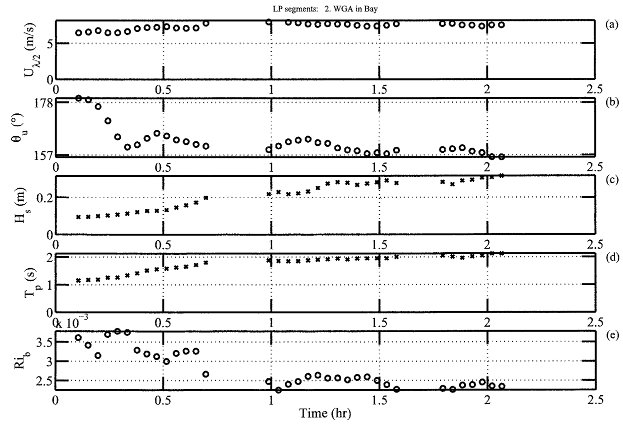

FIG. 4. Time series of (a) $U_{\lambda/2}$, (b) θ_u, (c) H_s, (d) T_p, and (e) Ri_b during the period of experiment.

sea stability condition is near neutral with the bulk Richardson number remaining mostly below 3.5×10^{-3}. The dimensionless parameters of t_*, e_*, and ω_* are calculated and listed in Table 3. There is some uncertainty on the initial time (t_0) of wind wave generation because the buoy is not in water at the beginning of the steady wind event. A trial and error approach is used to determine t_0; the detail is given in appendix B. Also, for the duration growth processing, we have used $U_{\lambda/2}$ as the scaling wind speed because $U_{\lambda/2}$ is a more meaningful property than U_{10} when addressing the dynamic coupling between atmosphere and ocean in the presence of surface waves. The calculated results of the dimensionless parameters using $U_{\lambda/2}$ and U_{10} are somewhat different. A more detailed discussion is presented in appendix C.

c. Results and discussions

The duration growth results are plotted in Fig. 5b together with datasets mentioned earlier (Sverdrup and Munk 1947; Bretschneider 1952a,b; Darbyshire 1959; DeLeonibus and Simpson 1972) and the ‘‘fully developed’’ wave measurements [in $e_*(t_*)$ only, peak wave periods are not available] reported by Moskowitz (1964). The results from the field experiment are in excellent agreement with the duration-limited growth functions converted from the fetch-limited empirical equations. The fetch-limited wave growth measurements (Burling 1959; Hasselmann et al. 1973; Donelan et al. 1985; Dobson et al. 1989; Babanin and Soloviev 1998) used to obtain the first- and second-order power-law fetch-limited growth functions (Table 1) are plotted in Fig. 5a for comparison. In general, the data scatter of duration-limited measurements is larger than that of the fetch-limited data, especially for the older datasets. As pointed out by one anonymous reviewer, for the present dataset, the first-order power-law functions converted from the fetch-limited growth curves seem to be in better agreement with measurements than the second-

TABLE 3. Duration-limited growth data from wave gauge array buoy deployment in St. Andrew Bay, FL.

Time (s)	U_{10} (m s^{-1})	$U_{\lambda/2}$ (m s^{-1})	θ_u (°)	H_s (m)	t_p (s)	10^3 Ri$_b$	t_*	$10^5 e_*$	ω_*
382	7.5	6.3	180	0.092	1.15	13.03	599	3.35	3.48
546	8.4	6.8	179	0.100	1.14	12.34	781	2.75	3.86
710	7.9	6.6	178	0.096	1.23	11.52	1054	2.90	3.45
873	8.3	6.8	172	0.105	1.19	12.78	1252	3.03	3.68
1037	6.9	6.0	162	0.111	1.34	13.03	1708	5.88	2.85
1201	7.9	6.6	159	0.108	1.25	12.58	1774	3.59	3.41
1365	8.6	7.3	160	0.122	1.43	11.20	1825	3.09	3.28
1529	8.3	7.2	165	0.136	1.56	10.65	2087	4.18	2.95
1693	8.1	7.0	166	0.127	1.55	10.31	2357	3.94	2.92
1856	8.6	7.4	166	0.124	1.56	9.86	2450	3.06	3.05
2020	8.6	7.5	162	0.148	1.63	10.25	2652	4.22	2.93
2184	7.3	6.5	162	0.167	1.68	10.38	3307	9.53	2.48
2348	8.3	7.3	164	0.161	1.65	10.22	3154	5.52	2.84
2512	8.5	7.6	158	0.192	1.82	8.31	3245	6.65	2.68
3558	9.4	8.5	160	0.243	1.95	7.65	4126	6.93	2.78
3722	8.8	7.8	160	0.221	1.90	7.07	4652	7.80	2.65
3886	9.3	8.2	163	0.227	1.76	7.53	4658	6.91	2.98
4049	8.6	7.7	165	0.209	1.91	7.73	5132	7.35	2.60
4213	8.5	7.6	162	0.234	1.90	8.11	5422	9.76	2.57
4377	8.6	7.6	164	0.257	1.85	8.16	5612	11.58	2.65
4541	8.4	7.6	160	0.266	1.96	7.91	5867	12.86	2.47
4705	8.7	7.8	161	0.302	1.95	7.87	5878	14.49	2.58
4869	8.4	7.5	159	0.281	1.92	7.78	6352	14.90	2.50
5032	8.4	7.5	158	0.256	1.88	7.91	6556	12.26	2.56
5196	8.2	7.4	160	0.267	2.04	7.93	6881	14.28	2.32
5360	7.9	7.1	155	0.304	1.94	7.63	7352	21.29	2.36
5524	8.5	7.6	159	0.276	1.89	7.31	7119	13.65	2.58
5688	8.5	7.7	158	0.298	2.04	6.92	7254	15.33	2.42
6457	8.5	7.8	159	0.260	2.08	6.92	8162	11.25	2.38
6621	8.5	7.7	160	0.292	2.04	6.89	8450	14.69	2.42
6785	8.7	7.8	159	0.262	1.92	7.25	8575	11.44	2.60
6948	7.9	7.1	160	0.320	1.96	7.21	9578	24.08	2.32
7112	8.2	7.6	156	0.303	2.20	7.37	9209	16.80	2.21
7276	8.1	7.3	158	0.298	2.00	7.00	9746	18.63	2.35
7440	8.3	7.6	155	0.326	2.19	6.97	9582	19.05	2.23

order power-law functions. It would be very interesting to see if similar outcome is repeated in future measurements. It is further noticed that many of the data points in the older datasets have dimensionless times up to an order of magnitude greater than the Pierson–Moskowitz limit. This may suggest that those points are either swell influenced or fetch limited and should be treated with caution. On the other hand, as shown in the figure, measurements by Moskowitz (1964) appear to reach the ‘‘fully developed’’ limit at the dimensionless fetch and dimensionless duration less than 10^4, which is considerably earlier than most other measurements. From the point of view of nonlinear wave–wave interaction, if the wind event is truly unlimited in fetch and duration, the wave spectrum undergoes continuous frequency downshift. As the characteristic wavelength increases, the capacity of the wave field to absorb atmospheric forcing increases and the mechanism of wave breaking that limits the wave growth becomes weaker. Under such a scenario, it is difficult to imagine that the wave growth should be limited (i.e., reaching full development). We feel that the concept of ‘‘full development’’ of a wave field deserves more critical examination and additional observations in the field are needed to establish or disprove the growth limit of wind-generated surface waves.

The wave gauge array data reported here expand the range (in terms of t_*) of the available duration-limited database by about one order of magnitude into the younger stage of wave development. As discussed earlier, both duration- and fetch-limited growth data can be expressed as $e_*(\omega_*)$, which represents the wave energy growth as a function of wave age and does not require the precise knowledge of wind fetch or wind duration. Figure 5c plots these two classes (fetch limited and duration limited) of data together. The development rate is clearly fetch/duration/wave-age dependent in both classes of data, and the fetch/duration/wave-age dependency is well represented by the second-order power-law functions. The agreement of these two classes of data presented in $e_*(\omega_*)$ also suggests the strong similarity of the ocean surface wave spectrum, as discussed by Young (1999) and others.

4. Summary and conclusions

Acquiring field measurements of duration-limited growth of wind-generated waves has always been a dif-

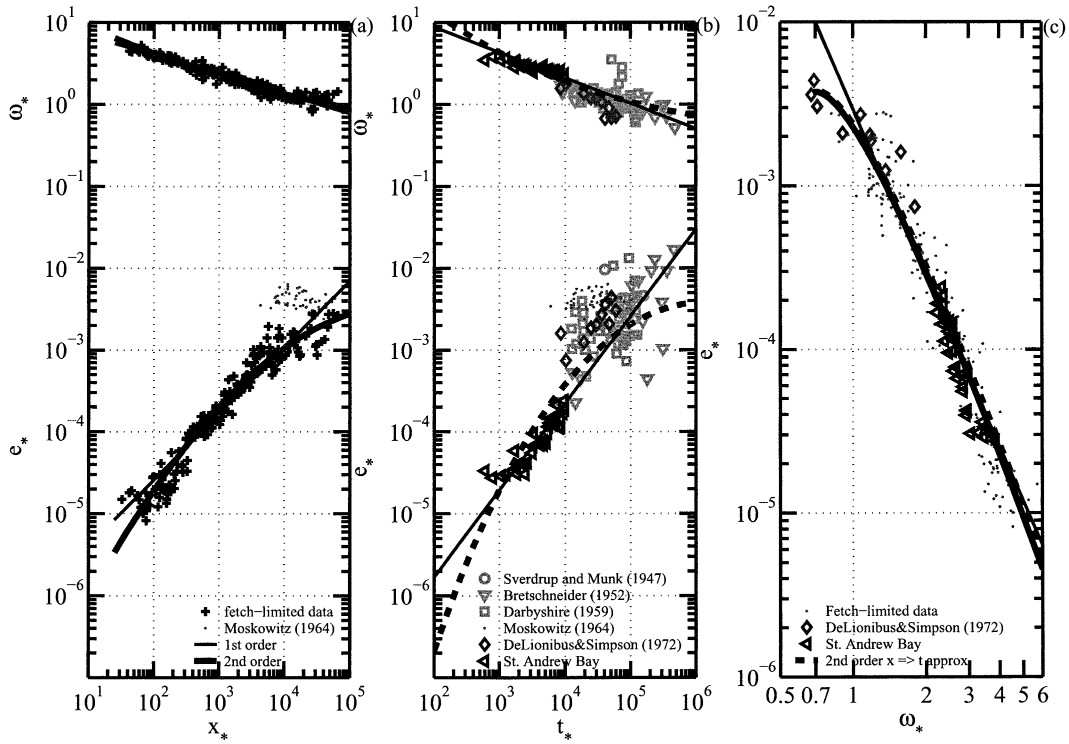

FIG. 5. As Fig. 1 but superimposed with experimental data.

ficult task. It is especially challenging to obtain duration growth data at young stage of wave development (Table 2). In comparison, over the years several field experiments on fetch-limited wind wave development have been successfully performed. These experiments collectively offer a coherent picture of the fetch-limited wave growth in terms of $e_*(x_*)$ and $\omega_*(x_*)$, which can be expressed as power-law functions (Fig. 5a). Using a higher-order data-fitting technique, the coefficients (A) and exponents (a) of the first-order (constant exponents) and second-order (fetch-dependent exponents) power-law functions are listed in Table 1. Through the connection of the group velocity, the fetch-limited growth functions (1–5) can be transformed to duration-limited growth functions (9–11). The computational results are shown in Fig. 1.

By chance, an almost ideal dataset of wind-generated surface waves in their first two hours of development is obtained. The location of the experiment is in a sheltered bay, so the background wave contamination is considerably smaller than that would have been possible in the open ocean. The measurements fill a big gap in our duration-limited database. The results are in excellent agreement with the duration-limited growth functions converted from fetch-limited growth functions (Fig. 5).

Acknowledgments. This work is sponsored by the Office of Naval Research (Naval Research Laboratory PE 61153N and 62435N). Our technicians Ray Burge, Dan Kennedy, Jeff Jones, and Mark Hulbert are responsible for the operation of the sophisticated scanning slope sensor and wave gauge array buoy. The captain and crew on board R/V *Longhorn* provided the critical logistics support. Nancy Mangin helped on data digitization and manuscript preparation. Two anonymous reviewers offered many insightful comments to improve the clarity and quality of the presentation. A large portion of the abstract of the revised version is extracted from the comments by one of the reviewers.

APPENDIX A

Space–Time Conversion

Figure 5a shows the scatterplots of $\omega_*(x_*)$ and $e_*(x_*)$ of the fetch-limited field measurements. The results can be represented by simple power-law functions (constant exponents) reasonably well for the fetch range $3 \times 10^2 < x_* < 10^4$. For a broader range of coverage, the development rate is obviously not constant based on examination of experimental data. Higher-order polynomial functions in log–log scales can be used to estimate the variable development rate. They also provide better agreement in the data trend between fitted functions and measurements, especially at very long and very short dimensionless fetches.

Using the following notations,

$$Y = \ln y \quad \text{and} \quad X = \ln x, \tag{A1}$$

the polynomial

$$Y = \sum_{n=0}^{N} \alpha_n X^n \tag{A2}$$

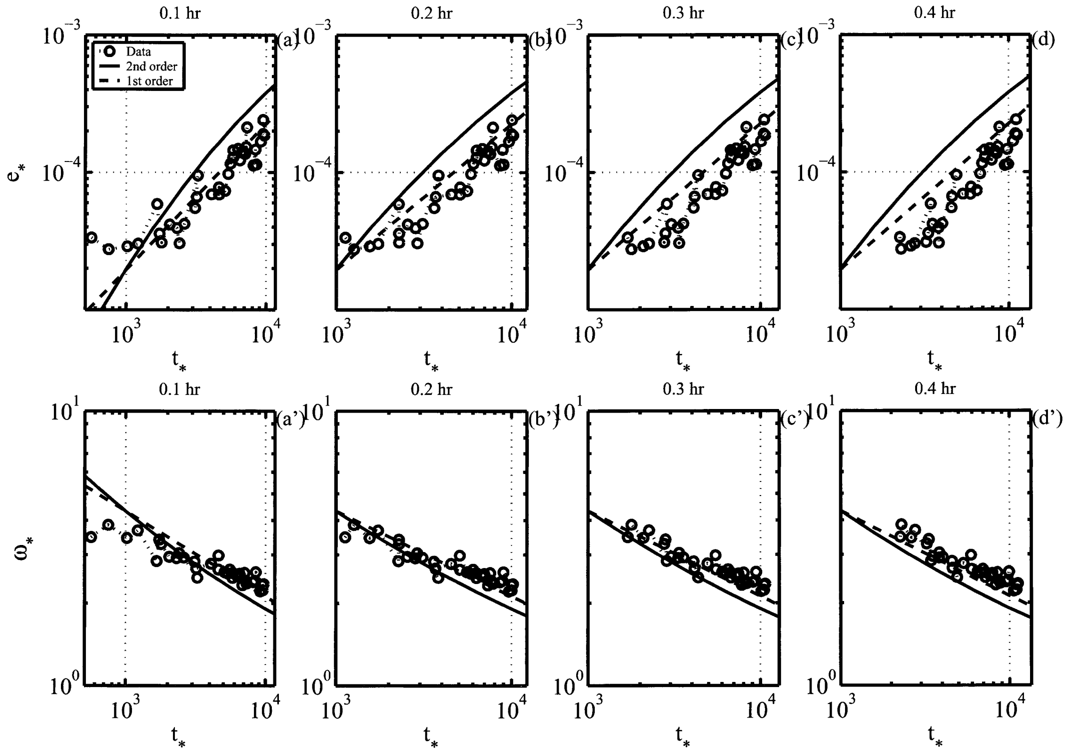

FIG. B1. Influence of the choice of starting time of wind event on the processed results of duration-limited wave growth. Examples of computations using different time lags (marked at the top of the panels) are illustrated.

is identically

$$y = e^{\alpha_o} x^{\sum_{n=1}^{N} \alpha_n (\ln x)^{n-1}}. \tag{A3}$$

For $N = 1$,

$$y = e^{\alpha_0} x^{\alpha_1} = A_{yx1} x^{a_{yx1}}. \tag{A4}$$

For $N = 2$,

$$y = e^{\alpha_0} x^{\alpha_1 + \alpha_2 \ln x} = A_{yx2} x^{a_{yx2}}. \tag{A5}$$

Note that $\alpha_1 + \alpha_2 \ln x$ is not the local slope of $y(x)$ for $N = 2$. Instead, the local slope should be evaluated by

$$\alpha_{yx} = \frac{x}{y}\frac{dy}{dx}, \tag{A6}$$

which yields

$$a_{yx2} = \alpha_1 + 2\alpha_2 \ln x \quad \text{and} \tag{A7}$$

$$A_{yx2} = e^{\alpha_0} x^{-\alpha_2 \ln x}. \tag{A8}$$

When applying the second-order solution (A5) to space–time conversion, the dimensionless frequency (dropping the asterisk subscript in all dimensionless variables here)

$$\omega = e^{\beta_0} x^{\beta_1 + \beta_2 \ln x} \tag{A9}$$

is substituted to (7) to arrive at

$$t = \int_0^x e^{\beta_0} x^{\beta_1 + \beta_2 \ln x}\, dx. \tag{A10}$$

With the change of variable $X = \ln x$ (A1), (A10) is transformed to

$$t = \exp(\beta_0) \int_0^{e^X} \exp[(\beta_1 + 1)X + \beta_2 X^2]\, dX, \tag{A11}$$

which leads to (see online at http://integrals.wolfram.com/index.en.cgi)

$$t = \frac{\exp[-(\beta_1 + 1)^2/4\beta_2]\sqrt{\pi}\, \mathrm{erf}i[(\beta_1 + 1 + 2\beta_2 x)/2\sqrt{\beta_2}]}{2\sqrt{\beta_2}}. \tag{A12}$$

To make use of (A12), the inverse solution expressing x as a function of t is needed for converting the fetch laws to duration laws. We are not successful in obtaining the inverse solution. Instead, the approximation ap-

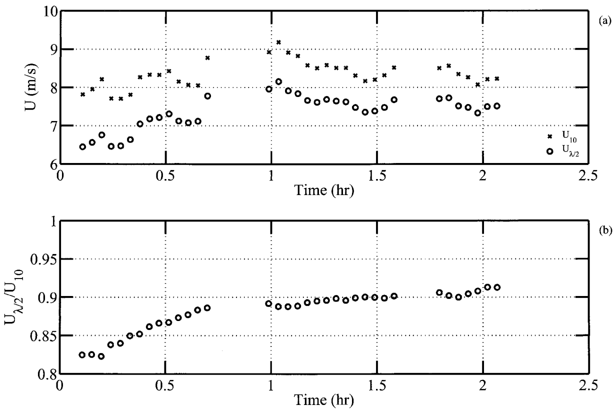

FIG. C1. Time series of (a) $U_{\lambda/2}$ and U_{10} and (b) the ratio $U_{\lambda/2}/U_{10}$.

proach substituting $A_{\omega x2}$, $a_{\omega x2}$, A_{ex2}, and a_{ex2} in (4)–(5) for $A_{\omega x}$, $a_{\omega x}$, A_{ex}, and a_{ex} in (8)–(11) is adopted. The results are satisfactory judging from the excellent agreement between the two $e_*(\omega_*)$ curves computed from fetch laws (solid curve) and the approximated duration laws (dashed–dotted curve) shown in Fig. 1c.

APPENDIX B

Determination of the Initial Time

Wave generation lags behind the wind event. The lag between starting times of the wind and waves is not known in the field environment. Data processing of the results of duration-limited growth may be influenced considerably by the choice of the initial time of the wind event. Because the buoy is not in water prior to wave inception, an absolute determination of initial time is not possible. In the absence of theoretical guidelines and the full history of the wind event prior to data acquisition, we process the measurements with several different starting time lags. Figure B1 shows several examples of the results. Because the relative error of measurements is large at the beginning stage of wave development, due to lower signal level and the presence of background wave motion (Fig. 2c), disagreement with the growth curve at the earlier stage is weighted less in the overall evaluation. The results tabulated in Table 3 use a time lag of 300 s for initiation of the wind event, judging from the field notes, which recorded that the buoy was released into water as soon as the ship anemometer indicated the start of steady wind and that the buoy system had a 5-min delay time for activating the data acquisition sequence. The tabulated time is the time at the middle of the short data segment referenced to this time lag. The data length of each segment is 4096/25 ≈ 164 s in time.

APPENDIX C

Parameterization with $U_{\lambda/2}$ and U_{10}

Conventionally, U_{10} is used as the scaling wind speed for the dimensionless parameters e_*, ω_*, x_*, and t_*.

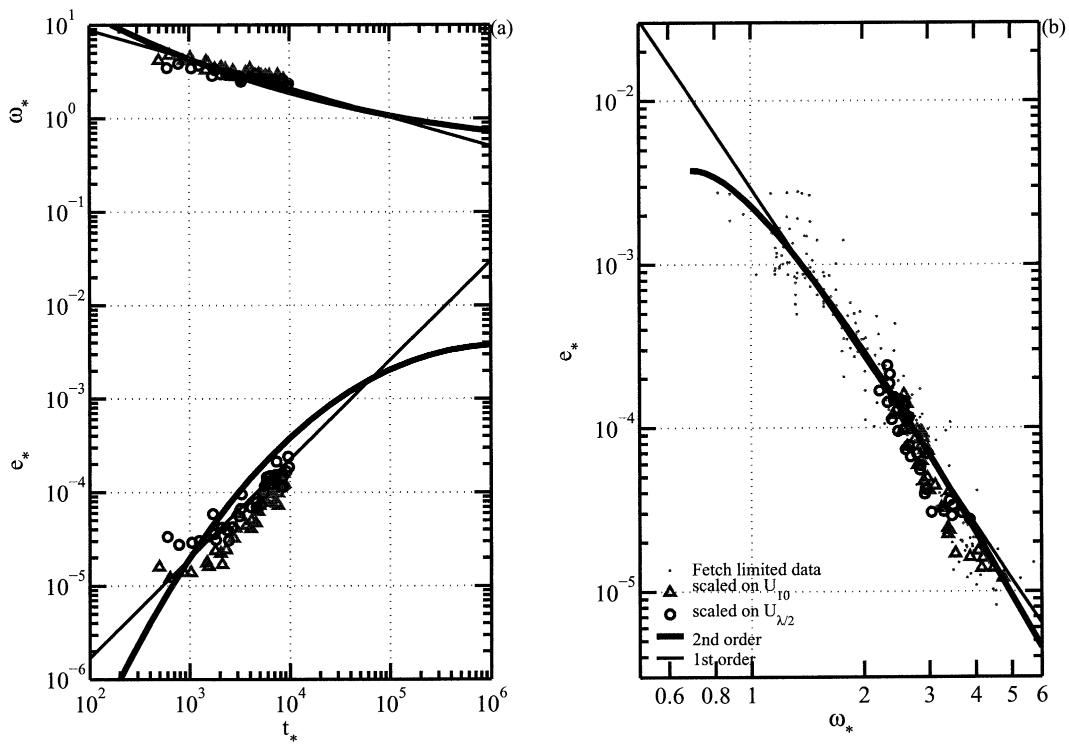

FIG. C2. Influence of the choice of scaling wind speeds on the processed results of duration-limited growth: (a) $e_*(t_*)$ and $\omega_*(t_*)$ and (b) $e_*(\omega_*)$. Fetch-limited data are also plotted in (b) for comparison with the duration-limited measurements.

Fixing the height for wind speed reference at 10 m is apparently based on operational or practical considerations rather than the dynamical significance of the 10-m elevation in the marine boundary layer. Because the influence of surface waves decays exponentially with distance from the interface and the wavelength is the vertical length scale of decay, the dynamically meaningful reference elevation should be the characteristic wavelength In the case of a water surface with multiple wave components, the representative wavelength is that of the component at the spectral peak, λ_p (e.g., Kitaigorodskii 1973; Stewart 1974; Donelan 1990; Hwang 2004). Of course, if the wind stress measurements were performed together with the wave growth experiment, the wind friction velocity u_* may serve as a better scaling wind velocity. All published fetch-limited growth data report e_*, ω_*, and x_* scaled with U_{10}. Conversion of U_{10} to u_* requires the application of the drag coefficient C_d. Presently, there are many equations for C_d; some take into account the wave age dependence and some do not. The issue is still under intensive debate, so scaling with $u.$ converted from U_{10} is not considered in this paper.

Quantitative differences are expected for the computed dimensionless parameters using different scaling wind speeds. Figure C1 plots the time series of the two wind speeds $U_{\lambda/2}$ and U_{10} and their ratio. Because the wave period for 20-m wavelength (under which condition $U_{\lambda/2} = U_{10}$) is about 3.58 s for deep water waves, for waves with periods shorter than 3.58 s, $U_{\lambda/2}$ is lower than U_{10}. The difference is more pronounced as the wave period deviates further from 3.58 s. For the present dataset, the average ratio $U_{\lambda/2}/U_{10}$ with one standard deviation is 0.88 ± 0.027.

The resulting $\omega_*(t_*)$, $e_*(t_*)$, and $e_*(\omega_*)$ using two different scaling wind speeds are graphed in Fig. C2. At the youngest stage of the present dataset, the dimensionless variance computed with $U_{\lambda/2}$ can exceed a factor of 2 higher than the value computed with U_{10}, and the dimensionless frequency (inverse wave age) is about 20% lower. While the difference is within the scatter of existing fetch-limited and duration-limited growth data [the fetch-limited results of $e_*(\omega_*)$ are plotted on the background in Fig. C2 for comparison], the scaling using $U_{\lambda/2}$ is adopted because $U_{\lambda/2}$ is dynamically more meaningful than U_{10}.

REFERENCES

Babanin, A. V., and Y. P. Soloviev, 1998: Field investigation of transformation of the wind wave frequency spectrum with fetch and the stage of development. *J. Phys. Oceanogr.,* **28,** 563–576.

Bretschneider, C. L., 1952a: Revised wave forecasting relationship. *Proc. 2nd Conf. on Coastal Engineering,* Houston, TX, ASCE, Council on Wave Research.

——, 1952b: The generation and decay of wind waves in deep water. *Trans. Amer. Geophys. Union,* **33,** 381–389.

Burling, R. W., 1959: The spectrum of waves at short fetches. *Dtsch. Hydrogr. Z.,* **12,** 96–117.

Chapman, R. D., and F. M. Monaldo, 1991: The APL wave gauge system. APL Tech. Rep. S1R-91U-041, The Johns Hopkins University, Laurel, MD, 32 pp.

Darbyshire, J., 1959: Further investigation of wind generated waves. *Dtsch. Hydrogra. Z.,* **12,** 1–13.

DeLeonibus, P. S., and L. S. Simpson, 1972: Case study of duration-limited wave spectra observed at an open ocean tower. *J. Geophys. Res.,* **77,** 4555–4569.

Dobson, F., W. Perrie, and B. Toulany, 1989: On the deep-water fetch laws for wind-generated surface gravity waves. *Atmos.–Ocean,* **27,** 210–236.

Donelan, M. A., 1990: Air–sea interaction. *The Sea,* B. LeMehaute and D. M. Hanes, Eds., Ocean Engineering Science, Vol. 9, Wiley Interscience, 239–292.

——, J. Hamilton, and W. H. Hui, 1985: Directional spectra of wind-generated waves. *Philos. Trans. Roy. Soc. London,* **A315,** 509–562.

Hanson, K. A., T. Hara, E. J. Bock, and A. B. Karachintsev, 1997: Estimation of directional surface wave spectra from a towed research catamaran. *J. Atmos. Oceanic Technol.,* **14,** 1467–1482.

Hasselmann, K., and Coauthors, 1973: Measurements of wind-wave growth and swell decay during the Joint North Sea Wave Project (JONSWAP). *Dtsch. Hydrogr. Z.,* **12** (Suppl. A8), 1–95.

Hwang, P. A., 2004: Influence of wavelength on the parameterization of drag coefficient and surface roughness. *J. Oceanogr.,* in press.

——, S. Atakturk, M. Sletten, and D. B. Trizna, 1996: A study of the wavenumber spectra of short water waves in the ocean. *J. Phys. Oceanogr.,* **26,** 1266–1285.

Kahma, K. K., 1981: A study of the growth of the wave spectrum with fetch. *J. Phys. Oceanogr.,* **11,** 1503–1515.

——, and C. J. Calkoen, 1992: Reconciling discrepancies in the observed growth of wind-generated waves. *J. Phys. Oceanogr.,* **22,** 1389–1405.

——, and ——, 1994: Growth curve observations. *Dynamics and Modeling of Ocean Waves,* G. J. Komen et al., Eds., Cambridge University Press, 74–182.

Kitaigorodskii, S. A., 1973: *The Physics of Air–Sea Interaction.* Israel Program for Scientific Translations, 237 pp.

Liu, W. T., K. B. Katsaros, and J. A. Businger, 1979: Bulk parameterization of air–sea exchanges of heat and water vapor including the molecular constraints at the interface. *J. Atmos. Sci.,* **36,** 1722–1735.

Mitsuyasu, H., and K. Rikiishi, 1978: The growth of duration-limited wind waves. *J. Fluid Mech.,* **85,** 705–730; Corrigendum, **87**, 796–797.

Moskowitz, L., 1964: Estimates of the power spectrums for fully developed seas for wind speeds of 20 to 40 knots. *J. Geophys. Res.,* **69,** 5161–5180.

Stewart, R. W., 1974: The air–sea momentum exchange. *Bound.-Layer Meteor.,* **6,** 151–167.

Sverdrup, H. V., and W. H. Munk, 1947: Wind, sea, and swell: Theory of relation for forecasting. Hydrographic Office Publication 60, U.S. Navy, 44 pp.

Wiegel, R. L., 1961: Wind waves and swell. *Proc. Seventh Conf. on Coastal Engineering,* The Hague, Netherlands, The Engineering Foundation, Council on Wave Research, 1–40.

Yefimov, V. V., and A. V. Babanin, 1991: Dispersion relation for the envelope of groups of wind waves. *Izv. Atmos. Oceanic Phys.,* **27,** 599–603.

Young, I. R., 1997: The growth rate of finite depth wind-generated waves. *Coastal Eng.,* **32,** 181–195.

——, 1999: *Wind Generated Ocean Waves.* Elsevier, 288 pp.

——, and L. A. Verhagen, 1996: The growth of fetch limited waves in water of finite depth. Part 1: Total energy and peak frequency. *Coastal Eng.,* **29,** 47–78.